A Communication-less Distributed Control Architecture for Islanded Microgrids with Renewable Generation and Storage

Aldana, Nelson Leonardo Diaz; Quintero, Juan Carlos Vasquez; Guerrero, Josep M.

Published in:
I E E E Transactions on Power Electronics

DOI (link to publication from Publisher):
10.1109/TPEL.2017.2698023

Publication date:
2018

Document Version
Accepted author manuscript, peer reviewed version

A Communication-less Distributed Control Architecture for Islanded Microgrids with Renewable Generation and Storage

Nelson L. Díaz, *Member, IEEE,* Juan C. Vasquez, *Senior, IEEE,* and Josep M. Guerrero, *Fellow, IEEE*

***Abstract*—For reliable operation of an islanded microgrid, at least one of its distributed resources should assume the responsibility of forming the off-grid power system. This responsibility is usually assumed by energy storage systems based on their capability of compensating the unbalance between generation and consumption. However, the storage units lose this capability when they reach the maximum and minimum limits of charge. Under these conditions, the regulation of the power grid may be assumed by another unit with enough capability or the power balance should be adjusted coordinately. This paper proposes a coordination architecture for islanded ac microgrids, which considers the appropriate charge profiles for battery-based energy storage systems. The architecture is based on distributed decision-making mechanisms, which use only local measurements for determining the operation mode of each unit independently. The coordination relies on a bus-signalling method, which enables the distributed units to have a global perception about the operation of the microgrid, without any communication infrastructure. The proposed architecture includes cooperative operation between distributed energy storage systems for achieving the equalization of the states of charge. Experimental results in a lab-scale microgrid with network configuration validate the proposed strategy under different operational conditions.**

***Index Terms*—Bus-Signalling, Coordinated control, Distributed energy resources, Droop control, Fuzzy adjustment.**

I. Introduction

THE use of variable renewable energy sources (RESs), such as photovoltaic (PV) and wind-turbine (WT) generators, has facilitated the electrification of remote sites such as telecommunication stations or small villages, thanks to the availability and low environmental impact provided by the primary energy resource [1]–[4]. However, The unpredictable nature of the RESs requires the use of complementary energy storage systems (ESSs) for smoothing their variations and provide enough energy back-up in the off-grid system. Here, the microgrid concept appears for defining a controllable and coordinate integration of different kinds of distributed energy resources (DERs) within a small-scale power system.

In particular, islanded microgrids imply additional challenges compared to grid-connected systems, since the voltage and frequency are not imposed by the utility grid. Therefore, the responsibility for forming the local power-grid should be assumed internally by at least one of the DERs [5]. Commonly, the ESSs assume this responsibility based on their inherent capability of absorbing/delivering energy for keeping the power balance in the islanded grid. Meanwhile, variable RESs are operated following algorithms of maximum power point tracking (MPPT) in order to make a more efficient use of the primary energy resource. Nevertheless, the storage devices have limited capacity and any charge or discharge beyond specified limits may result in their fast degradation or damage. Under extreme conditions of charge, the ESSs may not be able to continue ensuring the power balance and forming the local power-grid, as is the case of battery-based ESS, which requires specific charging stages for prolonging their lifespan.

In islanded microgrids, battery-based ESSs, and particularly lead-acid batteries are still the most used, since they offer a good commitment between deep-cycle life, transportability, availability, and cost [1], [2], [6], [7]. To prevent fast degradation of batteries, due to overcharge or deep discharge, a multi-stage charge profile is recommended by manufacturers in accordance with specific voltage limits. Normally, a second stage of charge is required in which the battery current is regulated for keeping the battery voltage in a constant value [7]. In that case, the ESSs will have to give up their role of forming the common bus in the islanded microgrid due to a change their operation mode [8]. Nevertheless, the regulation of the local grid may be assumed by another DER with enough capacity. Also, under deep-discharge conditions, the ratio between generation and consumption should be adjusted for avoiding further discharge. The aforementioned actions require a proper coordination between DERs and loads in order to keep the storage systems within safe operation limits and ensuring a reliable operation of the islanded microgrid.

The simplest way of enabling a reliable interaction between RESs and ESSs and ensuring safe operation of the storage devices is by keeping them within a partial state of charge (PSoC) as proposed in [9]. In this way, the ESS may keep the grid-forming operation continuously, since its maximum limits of charge and discharge are never reached. However, due to the unpredictable operation of RESs, the microgrid will require oversized storage devices. Centralized strategies can ensure the operation of the ESSs within safe ranges by means of a continuous communication with all the DERs. The central controller is able to dispatch the generation profiles of the DERs based on optimized functions, which penalizes the charge or discharge of the ESS beyond certain limits as in [10], [11], or by making that the ESS compensates only transitory mismatches between generation and consumption.

N. L. Díaz is with the Engineering Faculty, Universidad Distrital F.J.C., Bogotá 110231, Colombia (e-mail: nldiaza@udistrital.edu.co).

J. C. Vasquez, and J. M.Guerrero are with the Department of Energy Technology, Aalborg University, Aalborg 9220, Denmark (e-mail:juq@et.aau.dk; joz@et.aau.dk).

To do that, the generation from RES is adjusted until the power contribution from the ESS is restored to zero as in [12]. This fact results in an inefficient use of the primary energy resource and requires the integration of additional dispatchable sources. On top of that, the main drawbacks of centralized approaches are the dependence of the central control unit, which becomes a single point of failure in the coordination, and the use of dedicated communication channels, which are not always available for microgrids based on dispersed generators [13].

For distributed strategies, the interaction between units is commonly determined by the variation of the line frequency or voltage [14]. Normally, ac microgrids use the frequency instead of voltage, since the voltage is typically less accurate for signalling due to line impedances and reactive power flows. Meanwhile, dc microgrids rely mainly on voltage signalling. In [15], [16] ac microgrids based on a single PV generator and a battery-based ESS use multi-segments adaptive power/frequency (*P/f*) curves for enabling a seamless transition of the DERs between voltage control mode (VCM) and power control mode (PCM). The transitions are performed based on specific ratios between generation and consumption, instead of proper stages for charging the ESS based on batteries. Particularly in [15], the strategy requires additional droop controlled units for enabling the adaptive *P/f* behaviour. In [14] and [17], islanded microgrids based on a single (ESS + PV) configuration use a frequency bus-signalling strategy for avoiding that the storage system is charged or discharged beyond specific limits. Once the ESS reaches the limit of charge, a frequency pattern is generated by the ESS (operating as the grid-forming unit), which is recognized by the PV generator (operating in PCM) in order to adjust the generated power until it matches the power consumption such as in [17], or for turning off the PV generator such as in [14]. Four drawbacks can be highlighted in the approaches proposed in [14], [17]: (i) a slow inertia is required for adjusting the generation in the RES unit, which may cause than the charge go beyond specified limits. (ii) a full charge of the battery is not ensured since the battery current is set to zero when the threshold SoC value is reached. This fact may cause fast degradation of Lead-acid batteries [7]. (iii) the Lead-acid batteries are voltage limiting devices and their maximum limits should be defined by voltage levels instead of SoC values. The SoC value is commonly obtained from estimation methods which may be not accurate enough for ensuring safe operating limits [18]. (iv) the strategies have been considered for a single ESS. However, when the number of distributed ESSs increases, the definition of voltage and frequency patterns becomes difficult unless uniform charge profiles are ensured for all the distributed ESSs, or dedicated communication channels are used for enabling a perfect synchronization between units [14]. The last one is not a minor issue by considering that the current trend, is oriented to the use of distributed ESSs instead of a single ESS. In this way, each ESS can be optimized for the integration of new RESs [19], [20].

A coordination architecture for an islanded ac microgrids with distributed ESSs has been proposed in [21], which is based on seamless transitions between VCM and PCM in the DERs in accordance with particular operating conditions and a frequency bus-signalling method. This approach allows a faster transition between VCM to PCM for the ESSs, reducing the inertia that may cause overcharge in the storage devices. However, this architecture does not consider the different stages for charging batteries, actions for avoiding deep discharge of batteries, cooperative operation between ESSs, and does not present experimental results. Some coordination approaches for islanded dc microgrids have been considered recently in which the appropriate stages and transitions for charging distributed ESSs based on batteries are ensured, by means of centralized strategies as in [22], distributed strategies as in [23], and even by using power-line communication as in [24]. Nevertheless, coordination strategies with appropriate charging stages for distributed ESSs based on batteries are seldom explored for ac microgrids.

This paper proposes a fully distributed control architecture for coordinating the operation of variable RESs and distributed ESSs within an islanded ac microgrid. The DERs are self-controlled and coordinated by their own decision-maker (DM) units, who determines independently the operation mode and the way of interaction of each DER, relying only on local measurements and information. The DM units contain the set of rules and actions to be performed by each DER in accordance to their own particular conditions and global operating conditions of the whole microgrid. The rules which determine the interaction of the DERs are defined by a knowledge-based inference system deployed as finite state machines in the DM units. Therefore, the operating modes of each DER and the whole microgrid are limited within a finite number of operation modes, which look for ensuring the appropriate charging profiles for ESSs based on Lead-acid batteries, without losing the control over the regulation of the islanded microgrid. In order to eliminate the dependence on communication channels, the common bus by itself is used as the communication medium. In the proposed strategy, both voltage and frequency signals are considered for establishing a bus-signalling method, which contains the information required by the DM units for coordinating the operation of the DERs. The bus signals are generated independently by the units on the grid-forming control and this control can be alternated between different kinds of units. This fact allows a modular and expandable operation of the islanded microgrid. Apart from that, the proposed strategy includes cooperative operation between DERs based on adaptive power sharing functions for: (i) equalizing the SoC between distributed ESSs, which allows the distributed ESSs to have uniform charge profiles, allowing the definition of unified patterns of voltages or frequency within the signalling strategy. (ii) achieving an active power curtailment in the generation distributed RESs proportional to their own maximum capability, which enables an efficient use of the primary energy resource.

Section II defines the islanded microgrid and the main objectives of the proposed coordination architecture. Section III explains the different operational modes defined for a reliable operation of the islanded microgrid under different conditions. Section IV defines the different elements that configure the coordination architecture. Section V introduces cooperative behaviours for parallel connected grid-forming units. Section

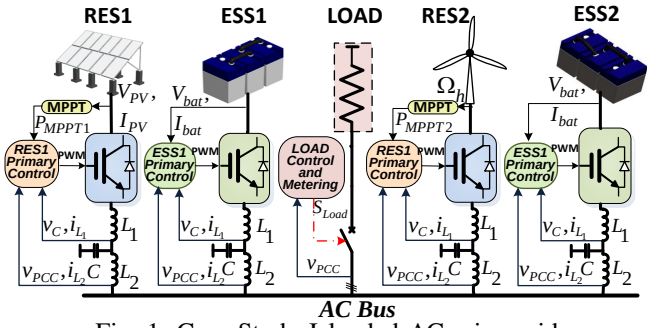

Fig. 1: Case Study Islanded AC microgrid.

VI presents the main parameters and characteristics of the low-voltage ac microgrid, in network configuration, which is used as a case study. Also, stability issues under different topological operation modes are considered in this section. Section VII shows experimental results and finally, section VIII presents conclusions.

II. Islanded Microgrid and Coordination Goals

A. Microgrid Structure

The network configuration of the islanded microgrid considered for this case study is shown in Fig. 1, in which the DERs and balanced loads are parallel connected in a common point of coupling. The microgrid is composed by two variable RESs (PV and WT), two distributed ESSs based on banks of valve regulated Lead-acid (VRLA) batteries, and a single load which represents an aggregation of distributed loads connected to the common bus through load switches. Nevertheless, the analysis can be scaled and expanded to microgrids with more DERs and loads. This is one of the inherent advantages of the proposed distributed architecture since it is highly modular and expandable. The DERs are interfaced with the ac grid by means of power electronic converters with LC filters (L_1 and C) and connected to the common bus through an output inductor (L_2) for emulating an inductive line impedance. Apart from that, each DER has its own primary controller, which enables autonomous operation of each unit based on specific operation modes [25]. Additionally, the load control and metering unit shown in Fig. 1 is responsible for generating the control signal (S_{Load}) for connecting or disconnecting the load based only on local measurements.

B. Coordination Goals

First, it is important to define the common goals of the microgrid, which will be the base of the coordination architecture. In this case, two main goals are defined:

1) The operation of the islanded power grid should be reliable and stable under different ratios of generation and consumption.
2) The appropriate stages for charging ESSs based on batteries should be ensured.

Based on the common objectives, it is possible to define the set of basic rules which will determine the interaction between the different DERs and loads in the islanded microgrid:

1) At least one DER has to assume the grid-forming control in order to ensure the regulation of the common bus and keep the power balance in the islanded power system.

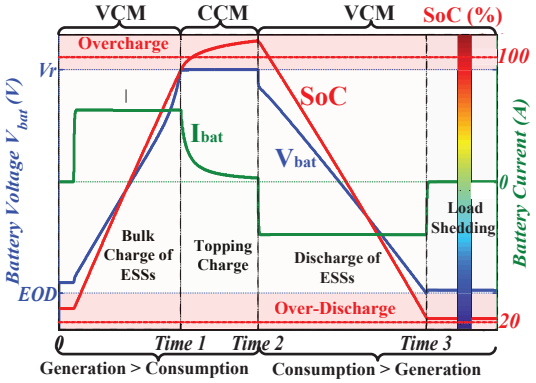

Fig. 2: Charging profile for Lead-acid batteries.

2) The grid-forming control should be alternated between ESSs and RESs based on their capacity and particular operating conditions as well as the operating conditions of the whole microgrid.
3) The RESs are more likely to operate following MPPT strategies in order to obtain from them the maximum amount of available energy. Because of that, they will only assume the grid-forming control when the ESSs are not able to continue storing energy.

C. Charging Profile of the Batteries

Lead-acid batteries are voltage limiting devices which cannot be charged or discharged beyond certain limits (typically defined by voltage values) under risk of degrading the performance or damaging the batteries. The values of the voltage thresholds are commonly defined by the manufacturers [7]. Additionally. Lead-acid batteries require full charge stages between cycles of discharge for avoiding sulfation of the plates, which is detrimental to the performance and capacity of the storage device [7], [26], [27]. Even if stages of full charge are not considered within discharge cycles, a periodic full charge should be scheduled as part of a proper maintenance of the batteries [9].

The best way of avoiding overcharge and at the same time ensuring a full charge of the batteries is by means of a two-stage charging procedure as shown in Fig. 2. The first stage (*0* to *Time 1* in Fig. 2) provides the bulk of the charge, while a second stage (*Time 1* to *Time 2* in Fig. 2) provides enough saturation to the battery charge by means of a topping charge procedure, in which the battery voltage (V_{bat}) is kept in a constant value. In this stage, the battery bank draws as much current as needed to keep regulated the battery voltage, which requires an appropriate current control [26]. Since the process of charging a battery is inefficient, it is necessary to return to the battery more than 100% of the energy, this excess of charge is provided during the saturation stage and typical values of overcharge may range from 5% to 30% [7], [27]. The regulation value (V_r), which defines the limit for the second stage of charge, is selected in accordance with the guidance from manufacturers, typically around 2.45 ± 0.05 volts/cell [7].

Similarly, the battery manufacturers recommend a threshold voltage value in which continuing with the discharge of the batteries will lead to a detriment in the performance of the

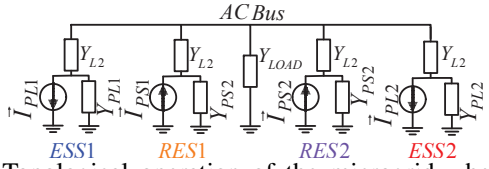

Fig. 3: Topological operation of the microgrid when all the DERs operate in CCM.

battery [7]. This value is known as the end-of-discharge (EOD) voltage. When the battery voltage reaches this limit, the load should be disconnected for avoiding further discharge of the ESSs as is shown in Fig. 2 at *Time 3*.

III. Operational Modes of the Microgrid

At the unit level, two basic operation modes can be assigned to the DERs in accordance to their primary control objective: (i) the voltage control mode (VCM) or grid-forming control, which will be assumed by the units responsible for forming, regulating and ensuring the power balance in the islanded power system. (ii) the current control mode (CCM) or grid-following control, which will be assumed by the units responsible for supplying or absorbing a specific amount of power [25], [28]. Different combinations of operation modes at the unit level represent different topological operating modes for the microgrid. In the proposed microgrid based on four DERs, all of them with two possible operation modes, 16 possible topological combinations (2^4) can take place. By taking into account the objective 1) and the rule 1) the combination in which all the units operate in CCM, as shown in Fig. 3, is not suitable since there is not any DER operating as grid-forming. In Fig. 3 the grid-following units operating in CCM are represented by an admittance in parallel with a constant current source. The grid-following units can be either power sources (PS) (supplying power) or power loads (PL) (absorbing power), which are differentiated by the sign of the current and the real part of the parallel admittance [29].

In accordance with rules 2) and 3), the grid-forming control should be alternated between ESSs and RESs, and the RESs will only assume the grid-forming control when batteries are not able to continue with the regulation. Because of that, topological combinations in which ESSs and RESs share the regulation of the power grid are not considered within the operation of the microgrid. This fact bounds the operation of the islanded system within six different combinations, which can be analyzed in four topological circuit modes (TCM) as shown in Fig. 4, where the grid-forming units are represented by a voltage source in series with an output admittance.

Figs. 4a and 4c show that some units can share the responsibility for the common bus regulation. In these cases, conventional $(P-\omega)$ and $(Q-E)$ droop controllers can be used for achieving good power sharing between grid-forming units, without additional communication [30]. To prevent coupling between active (P) and reactive (Q) power with respect to frequency (ω) and voltage amplitude (E) in resistive low-voltage microgrids, virtual inductances are commonly used [14], [21], [30]. Also, inductive lines can be added for interfacing the conversion stage and achieving the desired P-Q decoupling. In this case, the inductors L_2 (see

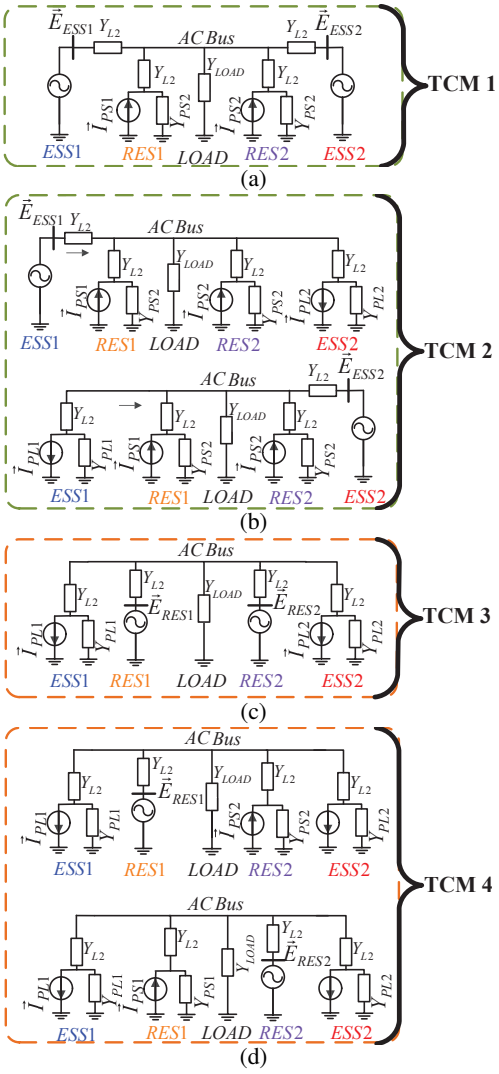

Fig. 4: Topological circuit modes for islanded microgrid.

Fig. 1) have been added for enabling the inductive line. The droop control loops adjust the frequency and voltage amplitude generated by the grid-forming units in order to achieve the appropriate active and reactive power sharing in accordance with the following equations:

$$\omega = \omega^* - K_p \cdot P_{uniti} \tag{1}$$

$$E = E^* - K_q \cdot Q_{uniti} \tag{2}$$

where, (E) is the output voltage amplitude of the i-th inverter, P_{uniti} and Q_{uniti} are the active and reactive power flow, E^* is the voltage amplitude reference, ω is the angular frequency of the output voltage, ω^* is the reference of the angular frequency, and K_p and K_q are the droop coefficients.

A. Topological Circuit Mode 1 (TCM1)

At this mode (Fig. 4a), all the distributed ESSs are grid-forming units, they are charged or discharged based on the unbalance between generation and consumption. The power is shared between ESSs by means of droop control loops. Meanwhile, RESs supply their maximum available power in accordance with the power reference imposed by their MPPT

algorithm. TCM1 also represents the operation of the microgrid under load shedding, in this case, the load admittance will be equal to zero $Y_{LOAD} = 0$.

B. Topological Circuit Mode 2 (TCM2)

This TCM considers the case in which one of the ESS has changed its operation mode (VCM to CCM) since the battery bank has reached the regulation value (V_r) and changes its operation to a topping charge stage. Under this stage, the behaviour of the ESS can be approximated by a power load (PL) as shown in Fig. 4b. Meanwhile, the other ESS is able to continue with the grid-forming control, since it still has the capacity to be charged.

C. Topological Circuit Mode 3 (TCM3)

In this case, all ESSs are under constant voltage charge (grid-following control). Then, RESs must assume the grid-forming control as can be seen in Fig.4c, providing that they have enough energy available to ensure the power balance of the power grid. In this case, droop control loops can also be used in order to share the power between RESs. Nevertheless, it is expected that the power participation of each RES will be proportional to its maximum power.

D. Topological Circuit Mode 4 (TCM4)

This TCM considers the case when the maximum available power from one of the RES falls below the power initially shared. Therefore, that RES returns to grid-following control. Meanwhile, the others RESs may still have enough capability to continue with the grid-forming control as can be seen in Fig.4d. The distributed RESs will continue moving from the VCM to CCM until the last one is not able to continue balancing the power in the islanded system. At this point, the microgrid should return to TCM1 and the batteries re-assume the regulation of the islanded power grid.

IV. Distributed Control Architecture

Once the TCMs of the microgrid have been specified for the different operating conditions, the next step is to define the events and conditions that will trigger the transitions between control modes at each DER. The coordination strategy should make decisions based on changing circumstances, and determine actions for adapting the operation of the distributed resources, complying with the common goals and rules. Since the proposed approach is completely distributed, the common bus voltage and local operating conditions at each DER are the only information available at each unit for determining the coordination actions. In general, to fulfil the objective 2) the transitions between control modes will be mainly determined by the proper charging stages of ESSs based on batteries.

A. Events for triggering transitions between control modes at each DER

1) Event 1 (Ev_1)*:* Represents the transition from VCM to CCM in ESSs, which is triggered once the battery arrays

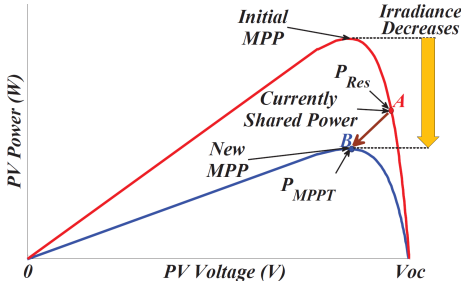

Fig. 5: The effect in the power generation from RESs when a RES initially working in VCM reduces its maximum power below the current shared power $(P_{MPPTi} < P_{Resi})$, (Ev_2).

reach the regulation value $(V_{bat} = V_r)$ as can be seen in Fig. 2 at *Time 1*. By considering differences in the SoCs between distributed ESSs, it is possible that one of the ESS continues in VCM while the other ESSs moves to grid-following operation as happening in Fig. 4b (TCM2). When the last ESS reaches the regulation value and changes its operation to CCM, the RESs should assume the grid-forming control. Consequently, the microgrid should change its topological operation to TCM3 in order to ensure a reliable operation.

2) Event 2 (Ev_2)*:* Represents the transition of the RESs from VCM to CCM, which is determined by the maximum available power at each unit. Since it is not possible to ensure that the distributed RESs keep the same maximum power during all the time, there may be the case in which the maximum power in a RES (P_{MPPTi}) drops below the current shared power (P_{Resi}), this is $(P_{MPPTi} < P_{Resi})$. This behaviour is illustrated in Fig. 5 for a PV generator, where a PV unit initially working off-MPPT (point ***A***) reduces its maximum available power due to a decrease in the solar irradiance (point ***B***). Then, the RES unit has to change its control to a grid-following mode and supplies its maximum available power. Nevertheless, the other RESs may have enough energy available to continue with the regulation of the common bus and the microgrid can operate in TCM4.

When the available power of the last RES in VCM is not enough to keep the power balance, it will return to CCM, since $(P_{MPPTi} < P_{Resi})$. Consequently, the ESSs (who are fully charged), may re-assume the grid-forming control.

3) Event 3 (Ev_3)*:* Activates the transition from CCM to VCM for all the DERs. Since the grid-forming control will be alternated between ESSs and RESs, this event occurs when the units that had been playing the role of forming the local grid (either ESSs or RESs) lose their capability of continuing with their forming role. This fact may be due to the change in the charging stage (Ev_1) in all the ESSs or because the generation from RESs is not enough to ensure the power balance (Ev_2). In both cases, the units that had been playing the grid-forming role change autonomously their operation from VCM to CCM as was explained in events Ev_1 and Ev_2. Therefore, for a short period, all the DERs will be in CCM and the microgrid will operate under the transitory topological circuit mode shown in Fig. 3, where there are not units responsible for forming the local grid. As a consequence, the frequency in the islanded power system (f_{ACbus}) will fluctuate, since the generation does not match the consumption. In this sense, the frequency

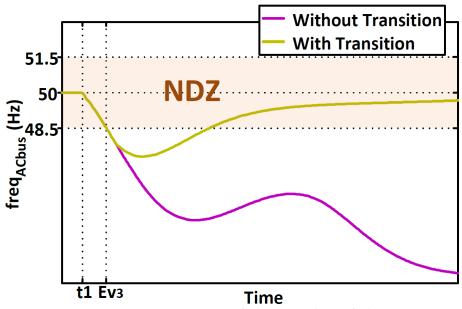

Fig. 6: Frequency response with and without transition between control modes after Ev_3.

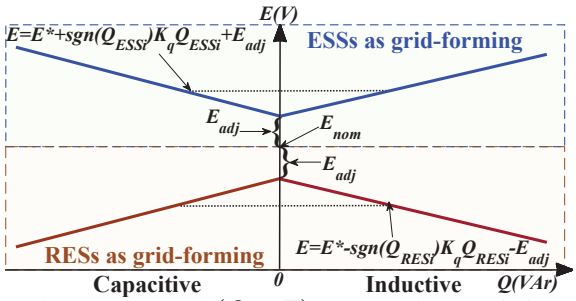

Fig. 7: Proposed $(Q-E)$ Droop Characteristics.

value can be used for signalling the transitions between CCM to VCM in the DERs. This kind of signalling strategy has been commonly used as a passive islanding detection method for triggering the transition of a microgrid between grid-connected to islanded operation [31], [32].

Since normal frequency fluctuations may appear when the load is added or removed, or when there is a change in the power injection of a DER, a Non-Detection Zone (NDZ) is defined [33]. The threshold limits of the NDZ cannot be set too small for avoiding transitions under normal frequency fluctuations but they should comply with international standards. The European Standard EN 50160 defines a frequency range of $\pm 2\%$ for an islanded system under normal operating conditions and allows a frequency range of $\pm 15\%$ under transitory conditions [34]. Because of that, the NDZ has been defined between a range of $\pm 3\%$ (48.5 to 51.1), in this way the normal fluctuations will not trigger any transition, and only transitory fluctuations beyond the NDZ will be considered for triggering the transitions. Nevertheless, the frequency fluctuations are kept within proper ranges.

When the frequency exceeds the threshold of the NDZ $(f_t = 50 \pm 3\%)$, the event Ev_3 is configured and a transition signal should be activated in the corresponding DERs (ESSs change to VCM when the RESs were the former grid-forming units or RESs change to VCM when the ESSs were the former grid-forming units). The Fig. 6 illustrate the expected frequency response when the proper transition is activated at Ev_3 after the microgrid changes to the transitory topological circuit mode of Fig. 3 at t_1.

The frequency is measured at each DER by means of synchronous reference frame Phase-Locked Loop (PLL) units, which have a very fast dynamic response and low overshoot under balanced grid conditions as the considered for this case study [28], [35], [36]. Nevertheless, the measured value of the frequency experiences a smooth transition when the grid frequency undergoes variations as is shown in [35]. This fact is particularly convenient for facilitating the detection of the threshold frequency at each DERs.

However, the event Ev_3 by itself does not provide enough information to the DERs about which kind of units should assume the grid-forming control, since during the transitory operation of Fig. 3, every DER will be in CMM. If only the Ev_3 is considered for triggering the transition between CCM to VCM, all the DERs will change simultaneously to VCM, which is against the rules 2) and 3). At this point, the challenge is to make that the right units assume the grid-forming control. Since the frequency is already used one possibility is to use the voltage amplitude for creating a voltage signature that allows the DERs to recognize which kind of units (ESSs or RESs) were the former grid-forming units.

B. Conditions for transitions based on voltage bus-signalling

In order to define a voltage signature for signalling purposes, when ESSs are the grid-forming units the voltage at the common bus will be set above the nominal voltage (E_{nom}). This fact is called condition (Co_1). On the other hand, when RESs are the grid-forming units the voltage amplitude at the common bus will be set below the nominal value (E_{nom}) (condition $\bar{Co}_1$). To achieve that, the conventional $(Q-E)$ droop control loops in (2) can be modified as:

$$E = \begin{cases} E^* + sgn(Q_{ESSi}) \cdot K_q \cdot Q_{ESSi} + E_{adj}, \\ \textbf{When } ESSs \textbf{ are } grid-forming; \\ E^* - sgn(Q_{RESi}) K_q \cdot Q_{RESi} - E_{adj}, \\ \textbf{When } RESs \textbf{ are } grid-forming. \end{cases} \quad (3)$$

where, (Q_{ESSi}) and (Q_{RESi}) represent the reactive power at each ESS and RES respectively, $(sgn(Q_{ESSi}))$ and $(sgn(Q_{RESi}))$ are sign functions for obtaining the nature of the reactive power (1 for inductive Q and -1 for capacitive Q). E_{adj} is an adjustment value added to the droop control loop for compensating the effect of the reactive current through the output inductor (L_2) on the voltage amplitude, at the point of common coupling (V_{PCC}). For instance, when the ESSs have the grid-forming control the voltage amplitude in the common coupling point (V_{PCC}) may become smaller than (E_{nom}) if the microgrid load is highly inductive. On the contrary, when the RESs have the grid-forming control the voltage at the common bus (V_{PCC}) may become bigger than (E_{nom}) if the microgrid load is highly capacitive. The value of E_{adj} can be estimated by considering the maximum reactive power (Q_{max}) and the voltage through the output inductor (L_2). The Fig. 7 illustrates the operation of the modified $(Q-E)$ droop control loop, which has been proposed for creating the voltage signature within the bus-signalling strategy.

C. Load Shedding based on voltage bus-signalling

When the generation from RESs is not enough to supply the load demand, the ESSs will be discharged for compensating the power unbalance while the microgrid operates in TCM1. Nevertheless, the ESSs cannot supply an unlimited amount of energy. As mentioned before, the battery manufacturers define

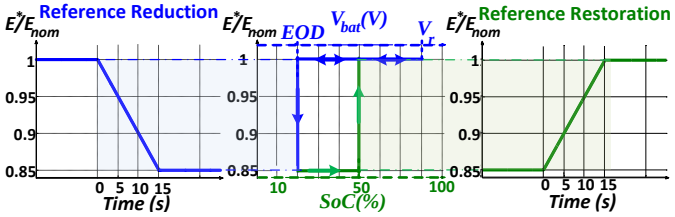

Fig. 8: Adaptive voltage pattern for load shedding.

a threshold voltage value (EOD in Fig. 2), for limiting the depth of discharge of the batteries. After the EOD value, the load should be disconnected from avoiding deep discharge [7].

To comply with the fully distributed approach, the control and measurement unit of the load should determine the connection/disconnection of the load relying only on local information. Because of that, the common bus should broadcast the information that the ESSs have reached the EOD value. Either voltage or frequency patterns could be used for triggering the load disconnection. However, reducing or increasing the frequency is not an option since frequency thresholds near the NDZ were already defined for alternating the grid-forming control between DERs. Because of that, a voltage pattern for the common bus has been proposed as shown in Fig. 8, this pattern is generated by the ESSs under grid-forming control.

Once the battery voltage reaches the EOD value in the ESSs, a new event (Ev_4) is configured. At this time, the reference value E^* in the primary controller of the ESS, will be reduced to a 15% of its nominal value (E_{nom}). The variation in the voltage reference will follow a linear behaviour with a negative rate of $-15\%/15s$ in order to get a smooth transition as shown in Fig. 8. Meanwhile, the local load control will recognize the variation in the voltage amplitude and will disconnect the load when the amplitude of the common bus voltage has dropped to a 10% of its nominal value. At this time the event (Ev_5) is configured and the load is disconnected.

On the other hand, the load can be reconnected when the voltage amplitude at the common point has been restored to a 90% of the nominal value E_{nom} $(\bar{E}v_5)$. The voltage reference will be restored to its nominal value when the SoCs of the ESSs become larger than 50%. This fact configures the event $((Ev_6))$ and the value of 50% is selected in order to provide a good operating margin to the ESSs for compensating any unbalance between generation and consumption. Similarly, for the voltage restoration process, a smooth transition in the voltage pattern is achieved by means of a positive rate of $15\%/15s$. Fig. 8 summarizes the behaviour of the proposed adaptive voltage pattern for load shedding and connection. In that figure, it is possible to realize that the disconnection of the loads is triggered by the voltage level as is recommend by the manufacturers, while the connection of the load rely on an estimated value of the SoC.

It is important to take into account, that the proposed strategy may have an important impact on the reactive power flow in the microgrid. this in the case that the ESSs do not reach the EOD value simultaneously, since the voltage reference E^* will be different at the each ESS. This fact may cause an increase in the reactive power managed by the ESS that reaches first the EOD value, which can rapidly exceed the rated capacity of the inverter. This issue can be solved by equalizing the discharge profiles of the distributed ESSs, which makes that the EOD value is reached almost at the same time in all of them. In this way, the proposed voltage pattern is uniformly generated by the distributed ESSs and an egalitarian reactive power sharing is kept. This particular behaviour will become clear later when the experimental results are shown.

TABLE I: Description of Events and Conditions

Event/Condition	Description
Ev_1	$V_{Bati} \geq V_r$
Ev_2	$P_{MPPTi} < P_{Resi}$
Ev_3	$f_{ACbus} \notin NDZ$
Ev_4	$V_{Bati} \leq EOD$
Ev_5	$V_{PCC} < 0.9E_{nom}$
Ev_6	$SoC_{bati} < 50\%$
Co_1	$V_{PCC} > E_{nom}$

TABLE II: Transition Tables for ESSs

Current Role	Input Ev_1	Input Ev_3	Input Co_1	Next Role	Output S_1	Output S_2
Grid-forming	1	X	X	Grid-following	1	0
Grid-following	X	1	0	Grid-forming	0	X

Current State	Input Ev_4	Input Ev_6	Next State	Output S_2
LC	1	X	LS	1
LS	X	1	LC	0

D. Distributed decision-makers

As exposed before, a reliable operation of the islanded power system can be ensured within a limited number of well-known topological operation modes. The islanded microgrid can continue operating in a specific topological circuit mode until some event causes a change in the control mode of a particular DER, which is reflected in a change in the TCM of the whole microgrid. In this sense, deterministic finite state machines (FSM) can contain all the information about the different events, transitions, and corresponding operation modes which should assume each DER in accordance to changing circumstances.

In order to comply with the distributed nature of the proposed coordination approach, independent decision-making (DM) units based on FSM will be deployed at each DER. Since the events and conditions for triggering the transitions between operation modes differ for ESSs, RESs, and loads, the FSM at each DM should be designed to fit with the nature of the corresponding unit. Table I summarizes the events (Ev_i) and conditions (Co_i), which are the input of the FSMs.

The decision-maker for ESSs is a hierarchical FSM with two states at the higher level for defining the control mode of the ESSs (grid-forming or grid-following), and two states in a lower level inside the grid-forming state (load connected (LC) and load shedding (LS)). The decision-maker has two outputs (S_1) and (S_2) which are the signal for enabling the transitions between the control modes of the ESSs and for defining the voltage reference respectively. Fig. 9a illustrates the state diagram for ESSs and Table II shows the corresponding transition tables for ESSs.

In the case of RESs, a FSM with two states and one output is enough for enabling the two control operation modes (grid-forming ($S_1 = 0$) or grid-following ($S_1 = 1$)). The Fig. 9b

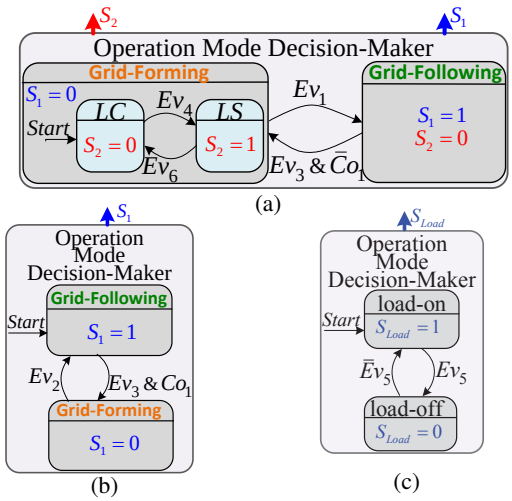

Fig. 9: Decision-Making units based on FSM for (a) ESSs, (b) RESs, and (c) Loads.

TABLE III: Transition Table for RESs

Current Role	Input Ev_2	Input Ev_3	Input Co_1	Next Role	Output S_1
Grid-following	X	1	1	Grid-forming	0
Grid-forming	1	X	X	Grid-following	1

shows the state diagram for RESs and the Table III shows its corresponding transition table. Similarly, Fig. 9c and Table IV show the state diagram and the transition table for the load control, which has two possible states defined by one output (load-on ($S_{Load} = 1$) and load-off ($S_{Load} = 0$)).

V. Cooperative Operation Between Grid-Forming Units

Within the proposed distributed architecture, it is possible to define cooperative behaviours between parallel connected grid-forming units. For instance, ESSs can adjust their power participation in order to balance the stored energy (SoC equalization) and ensure similar charging profiles for the distributed ESSs. Similarly, RESs can adjust their shared power proportionally to their maximum available power.

A. Stored Energy Balance Between ESSs

The SoC equalization consists on equalizing the charging profiles for the distributed ESSs. This procedure brings additional advantages to the overall performance of the whole microgrid such as: i) reducing the uneven degradation of the distributed banks of batteries, ii) speeds-up the charge of all the distributed ESSs, and iii) allows a smooth transition between operation modes for distributed ESSs, since the different charging stages are achieved almost simultaneously for the distributed ESSs [37].

Commonly, for performing the SoC equalization the conventional $(P - \omega)$ droop control loops defined by (1) are complemented with adaptive strategies that modify or weight

TABLE IV: Transition Table for Load Control

Current State	Input Ev_5	Next State	Output S_{Load}
load-on	1	load-off	0
load-off	0	load-on	1

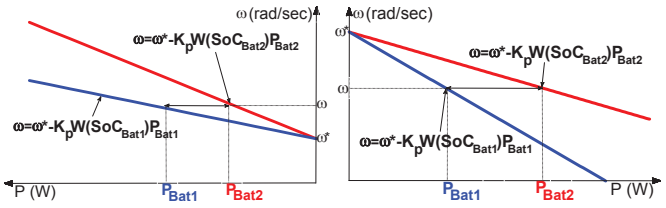

Fig. 10: Active power sharing with weighted droop coefficients for: (a) ESSs charge, (b) ESSs discharge.

the droop coefficient (K_p in (1)) in accordance to the differences in the SoC values. In this way, the proportion of power shared by each ESS is modified and consequently, the rates of charge and discharge can be adjusted for ensuring the equalization. In this sense, different strategies based on communication networks have been proposed for dc and ac microgrids such as in [38]–[41], which adjusting the value of the droop coefficients based on global information. Also, distributed SoC equalization approaches without any communication, applied mainly to dc microgrids, have been proposed in [13], [42], which weight the droop coefficient in accordance to adaptive charge and discharge curves obtained from exponential functions of the SoC. In general, those kind of adaptive curves are complex to tune and difficult to adapt for ac microgrids due mainly to stability constraints and that independent functions are required for the charging and discharging process [13], [29].

The basic idea behind the adaptive curves, is to obtain a SoC-dependent weighting function ($W\left(SoC_{Bati}\right)$) for weighting the droop coefficient K_p at each ESSs. Then, equation (1) can be re-written as:

$$\omega = \omega^* - K_p \cdot W\left(SoC_{Bati}\right) \cdot P_{Bati} \tag{4}$$

During the SoC equalization, it is expected that the ESS with the lowest SoC is charged faster. This can be achieved by setting a smaller value in the product $(W\left(SoC_{Bati}\right) \cdot K_p)$, which in turn increases the amount of power shared (P_{Bati}) by that ESS. On the opposite, a larger value in the product $(W\left(SoC_{Bati}\right) \cdot K_p)$ is required for reducing the amount of power shared by the ESS with the lowest SoC, during the process of discharge. To illustrate, Fig. 10 show the effects in the shared power by adjusting the weighting factor in the case that $(SoC_{Bat2} > SoC_{Bat1})$ for charge and discharge. In Fig. 10a, $|P_{Bat1}| > |P_{Bat2}|$, since $(W\left(SoC_{Bat1}\right) < W\left(SoC_{Bat2}\right))$. Meanwhile, in Fig. 10b $|P_{Bat2}| > |P_{Bat1}|$, since $(W\left(SoC_{Bat1}\right) > W\left(SoC_{Bat2}\right))$. As an alternative, knowledge-based fuzzy inference systems (FIS) can be used for obtaining the adaptive functions of the weighting factor $(W(SoC))$. This kind of approaches have been deployed previously for dc microgrids in [23], and since the adaptive curves are synthesized from qualitative knowledge without considering particular parameters of the storage devices or the microgrid, they can be easily adapted for ac microgrids. The inputs of the FIS are the SoC and the sign of the power at each ESS $(sgn(P_{Bati}))$, which provides the information about the charging or discharging status of the ESSs. Figs. 11a and 11b show the profile of the control curves for the adaptive

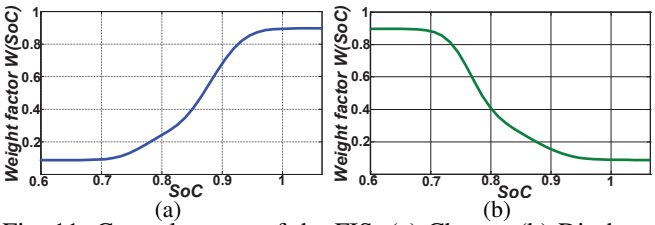

(a) (b)

Fig. 11: Control curves of the FIS: (a) Charge, (b) Discharge.

weighting factor $(W(SoC))$ under charge and discharge. Each ESS has its own fuzzy system for obtaining locally the weighting factor $(W(SoC))$ based on it own SoC. The SoC is estimated by the ampere-hour (Ah) counting method [7], [17]. Nevertheless, any other estimation method can be used. An inherent advantage of using the FIS is that the curves are normalized, which allow selecting the nominal value of the droop coefficient K_p in accordance with operational or stability constraints.

B. Power Curtailment of RESs under Grid-Forming Operation

RESs assume the bus regulation when ESSs are not able to store more energy (ESSs are under constant voltage regulation), and the maximum power of RESs is larger than the current power consumption (TCM3). At this point, the power balance is shared between distributed RESs by means of conventional droop control loops (eq. (1)) and the generation from RESs should be curtailed for keeping the power balance in the system. However, it is no possible to ensure that all the distributed RESs have the same maximum power (P_{MPPT}), therefore an equal sharing is not always feasible. Under this context, it is expected that the RES with more available power contributes with more power than the others. Therefore, the contribution of each RES in the power sharing may be adjusted by means of a weighting factor $(W(P_{MPPT}))$ in its droop control loop. Then, equation (1) is modified as:

$$\omega = \omega^* - K_p \cdot W(P_{MPPT}) \cdot P_{Resi} \tag{5}$$

where, P_{Resi} is the actual value of the power supplied by each RES under grid-forming operation.

Taking into account that the proposed control architecture is completely distributed, the weighting factor $(W(P_{MPPT}))$ should be obtained only from local measurements. By regarding that the value of the weighting factor must be inversely proportional to the maximum power, it is defined as:

$$W(P_{MPPT}) = P_{base}/P_{MPPTi} \tag{6}$$

where, P_{base} is selected in accordance with the maximum power rate of the RESs [23]. However, the value of the $(W(P_{MPPT}))$ should be bounded in order to avoid undesired dynamic response of the microgrid. This fact will become clear later when stability issues are considered.

VI. Case Study Islanded Microgrid

Table V summarizes the main parameters of the microgrid in network configuration selected for the case study. The islanded microgrid was initially dimensioned with a battery capacity of 10 Ah in each ESSs. However, in order to speed up the experiments, the capacity of batteries is set at 0.016 Ah. The batteries are modelled by means of detailed aggregated models, which take into account the fast and slow dynamic responses, and the output series resistor of the battery array [43], [44]. For emulating the active power consumption in the microgrid a resistive load will be considered.

TABLE V: Parameters of the Microgrid

Parameter	Symbol	Value
Power Stage		
Nominal Voltage	E_{nom}	$120 * \sqrt{2}$ V
Voltage Adjustment	E_{adj}	3 V
Nominal Frequency	ω^*	$2 * \pi * 50$ rad/s
Threshold Frequency values	f_t	$50 \pm 3\%$ Hz
Inverter and line inductors	L_1, L_2	1.8 mH
Filter Capacitor	C	27μF
Loads	P_{Load}	366 W, 188 W
Maximum Reactive power flow	Q_{max}	$\pm$1500 VAr
Battery Array		
Nominal Voltage	V_{Bat}	420 V
End-of-discharge Voltage	LVD	400 V
Regulation Voltage	V_r	432 V
Nominal Battery Capacity	C_{bat}	10 Ah
Power Flow Control		
ESS $(P-\omega)$ Droop Coefficient	K_{pESS}	$5.61 * 10^{-5}$ (rad)/(s)/(W)
RES $(P-\omega)$ Droop Coefficient	K_{pRES}	$1.61 * 10^{-5}$ (rad)/(s)/(W)
$(Q-E)$ Droop Coefficient	K_q	$1 * 10^{-3}$ V/(VAr))
P_{base} for $W(P_{MPPT})$ calculation	P_{base}	100 (W)
Reactive power Reference	Q^*	0 VAr
Cut-off frequency (measurement filter)	ω_f	6.28 (rad)/(s)

A. Implementation of distributed primary controllers

Figs. 12 and 13 show the scheme of the primary controllers for the ESSs and RESs respectively. The primary controllers are presented by means of functional blocks, which include the inner current control loops and outer voltage control loops, the proposed $(P-\omega)$ and $(Q-E)$ droop control loops, the measurement block, and the operation mode decision-maker. The current control loop is the same for CCM and VCM, then, a smooth transition between control modes is achieved by setting the initial conditions of inactive PI controllers to the current value of the reference current. In this way, same conditions are ensured before and after the transitions, which avoids discontinuities at the reference current. The operation mode decision-making units presented on Fig. 9 generate the signals for activating the transitions between control modes. The reactive power Q will be managed and shared exclusively by the grid-forming units, then, the reactive power reference (Q^*) is set equal to zero for the grid-following units.

B. Stability Considerations

The stability of the microgrid relies mainly on the grid-forming units. Therefore, their inner and outer controllers have been designed to provide active damping to the inverters grid side converters. The dynamic behaviour of the microgrid with parallel connected grid-forming units depends mainly on the interaction of the droop control loops, since the references for the sinusoidal voltage amplitude (E) and frequency (ω) in the grid-forming units are obtained directly from them [45]. Particularly, the nominal values of the droop coefficients (K_p and K_q) determine the dynamic behaviour of the islanded

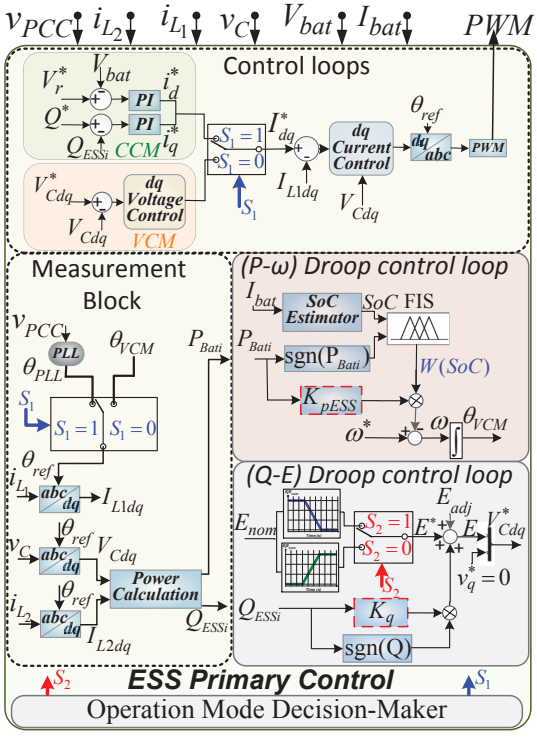

Fig. 12: Scheme of the primary control for ESSs.

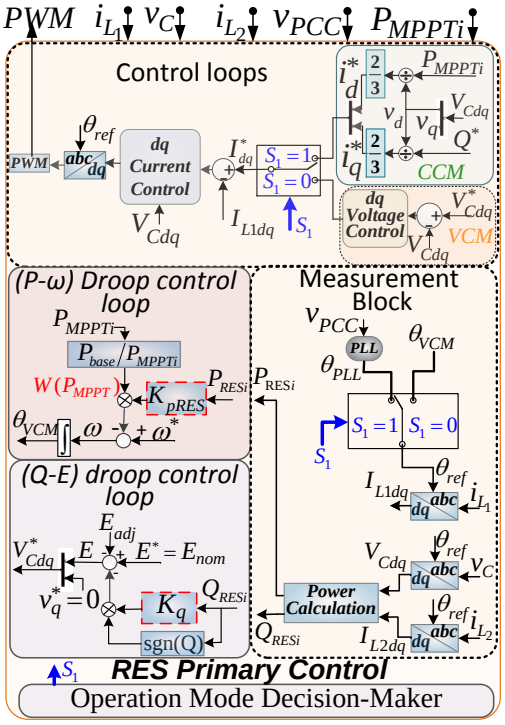

Fig. 13: Scheme of the Primary control for RESs.

system [29]. The small signal model of a single grid-forming unit can be obtained after linearising the equations (1) and (2) as proposed in [45]:

$$\begin{bmatrix} \Delta\dot{\omega}_i \\ \Delta\dot{v}_{di} \\ \Delta\dot{v}_{qi} \end{bmatrix} = [M_i] \begin{bmatrix} \Delta\omega_i \\ \Delta v_{di} \\ \Delta v_{qi} \end{bmatrix} + [C_i] \begin{bmatrix} \Delta P_i \\ \Delta Q_i \end{bmatrix} \tag{7}$$

where, the state variables are the small deviation around the equilibrium point of the output frequency $(\Delta\omega)$ and voltage $(\Delta v_{di}$ and $\Delta v_{qi})$, by considering a $d-q$ reference frame in which $(\vec{E} = v_d + jv_q)$. For a microgrid composed by several grid-forming units connected in parallel, and considering the integration of power sources (PS), power loads (PL) and the line impedances within the microgrid network, it is possible to obtain a more detailed small signal model, which symbolically can be written as:

$$[\Delta\dot{X}] = ([Ms] + [Cs]([Is] + [Es][Ys])[Ks])\,[\Delta X] \tag{8}$$

$$+[Cs][Es][Hs][\Delta i_{P(S-L)}]$$

where, $[Ys]$ and $[Hs]$ are the nodal admittance matrix and the forward current gain matrix of the microgrid network respectively, $[Is]$ and $[Es]$ are matrices with the values of current and voltages in the equilibrium point for the grid-forming units, $[\Delta i_{P(S-L)}]$ is the incremental current from the power sources and loads, and $[Ks]$ is a transformation matrix for making $([\Delta E] = [Ks][\Delta X])$. Interested readers about the parameters of the matrices may refer directly to [29].

Fig. 14a shows the behaviour of the eigenvalues for the microgrid under TCM1 and TCM3 (two parallel connected grid-forming units), by varying the droop coefficient (K_p) from $5.60 * 10^{-6}$ to $5.04 * 10^{-5}$ rd/s/W and by keeping the

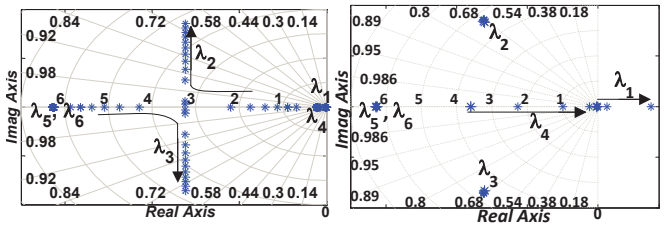

(a) (b)

Fig. 14: Root Locus plot for TCM1 and TCM3 varying: (a) K_p, (b) K_q.

value of (K_q) constant. For the defined range, the system has a resonant mode whose damping ratio (ζ) decreases when (K_p) is increased. In this case, a minimum damping ratio $(\zeta = 0.707)$ has been considered as acceptable for ensuring stable dynamic response of the system. Because of this, the maximum value for the $(P-\omega)$ droop coefficient is $(K_{p(max)} = 5.61 * 10^{-5} rd/s/W)$. For the ESSs the product $(W\,(SoC_{Bati}) \cdot K_p(max))$ is approximately bounded to the selected maximum value, since the $(W(SoC))$ vary between 0.1 to 0.9 as can be seen in Fig. 11. Then, a nominal value $(K_{pESS} = 5.61 * 10^{-5} rd/s/W)$ is established for ESSs. For RESs, the nominal value of the $(P-\omega)$ droop coefficient is established at $(K_{pRES} = 1.61 * 10^{-5} (rad)/(s)/(W))$ and consequently $(W(P_{MPPT}))$ should be limited to 5 for do not exceed the value of $K_p(max)$.

Fig. 14b shows the behaviour of the eigenvalues of the microgrid under TCM1 and TCM3 by varying the $(Q-E)$ droop coefficient (K_q) from $1 * 10^{-3}$ to $3 * 10^{-3} V/(VAr)$ and by keeping the $(P-\omega)$ droop coefficient (K_p) on the maximum value. In this case, the system becomes unstable

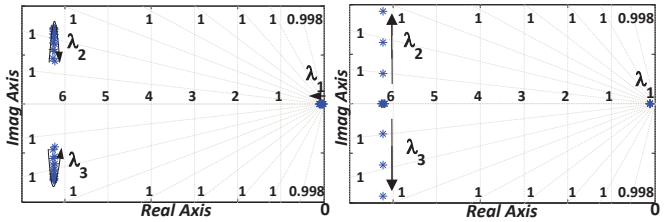

(a) (b)

Fig. 15: Root Locus plot for TCM2 and TCM4 varying: (a) K_p, (b) K_q.

for $K_q \geq 2.3 * 10^{-3} V/(VAr)$. Therefore, the nominal value of the $(Q - E)$ droop coefficient is selected at $(K_q = 1 * 10^{-3} V/(VAr)))$. Whit this value it is possible to estimate the maximum voltage deviation:

$$\Delta E = K_{qRES} \cdot Q_{max} + E_{adj} \tag{9}$$

where, $(E_{adj} = 3V)$. This value was selected by taking into account that the voltage drop in the output inductor L_2 will be approximate $\pm 3V$ in the case that $(Q = Q_{max})$. Therefore, under normal operation (load connected) $\Delta E < 0.05 E_{nom}$ as recommended by different grid codes.

Similarly, Figs. 15a and 15b show the behaviour of the eigenvalues for the microgrid under TCM2 and TCM4, by varying K_p and K_q respectively. As can be seen, the stability of the system is not compromised with the selected values of the droop coefficients.

Once the right nominal values of the droop coefficients have been selected for ensuring a stable operation of the microgrid, it is important to determine the local asymptotic stability of the equilibrium points, which ensure that all initial conditions after the transitions in the operation modes will result in trajectories that converge to the equilibrium points. In this sense, it is possible to determine the local stability of an equilibrium point by means of a linear approximation [46]. Then a linear system will be derived for evaluating the local asymptotic stability of the grid-forming units under different initial conditions.

Since the generated voltage is aligned to the synchronous frame, the quadrature component of the voltage $(v_q = 0)$. Therefore, the instantaneous active and reactive power are:

$$P_i = \frac{3}{2}\left(v_{di} i_{di}\right) \tag{10}$$

$$Q_i = \frac{3}{2}\left(v_{di} i_{qi}\right) \tag{11}$$

and the values obtained after the power calculation block are:

$$P_{meas}(s) = \frac{\omega_f}{s + \omega_f} P_i(s) \tag{12}$$

$$Q_{meas}(s) = \frac{\omega_f}{s + \omega_f} Q_i(s) \tag{13}$$

where, ω_f is the cut-off frequency of the measuring filter. By replacing the equations (12) and (13) in equations (1) and (2), and after linearisation at the equilibrium point $(v_{di}, i_{di}, i_{qi}, \omega)$, it is possible to obtain the linear approximation as:

$$\begin{bmatrix} \Delta\dot{\omega}_i \\ \Delta\dot{v_{di}} \end{bmatrix} = \begin{bmatrix} -\omega_f & -\frac{3}{2} k_p \omega_f i_{di} \\ 0 & -\omega_f (1 + \frac{3}{2} k_q i_{qi}) \end{bmatrix} \begin{bmatrix} \Delta\omega_i \\ \Delta v_{di} \end{bmatrix} \tag{14}$$

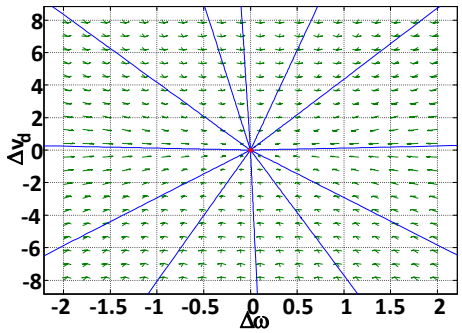

Fig. 16: Phase portrait for the linear approximation system in equation (14).

It is straightforward to verify that the real parts of all eigenvalues of equation (14) are strictly less than zero (as occur also for the linear system in equation (8)), then, the equilibrium point of the linear approximation is asymptotically stable. By considering that, "*the asymptotic stability of the linear approximation implies 'local' asymptotic stability of the original non-linear system*" [46]. It is possible to have an insight into the local asymptotic stability of the islanded microgrid after the transitions, mainly by considering that the deviations in voltage and frequency are kept within a 5% of the nominal values.

It is possible to perform a qualitative analysis of the evolution of the voltage amplitude E and frequency ω during the transitions in operation modes by plotting the phase portrait for the system in equation (14) (Fig. 16). This tool provides an insight into the dynamic behaviour of the microgrid by showing the trend of different trajectories under different initial conditions [46]. As can be seen in Fig. 16 all the trajectories converge to the equilibrium point.

VII. Experimental Results

The performance of the case study microgrid with the proposed coordination architecture was tested experimentally in an islanded ac microgrid laboratory platform. Fig. 17 shows a scheme of the experimental setup, which can be divided into two parts. The hardware part is composed of four inverters Danfoss (2.2 kW), LCL filters, measurement LEM sensors, and a resistive load. Meanwhile, the software part is implemented in a real-time simulation platform (dSPACE1006 control board), where the controllers, battery models, and renewable generation profiles are emulated. For the integration of RESs to a energized grid, it is commonly used a multi-stage converter in which one of the converters is responsible for the regulation of an intermediate dc-link, while the other follows the power reference obtained from the MPPT algorithm such as in [47]. In the experimental configuration, the MPPT reference (P_{MPPTi}) is directly applied to the grid side converter, which is connected to a stiff voltage source that emulates the intermediate dc-link as can be seen in Fig. 17. Fig. 18 shows an image of the experimental setup.

A. Experiment 1.

Fig. 19 shows the experimental performance of the microgrid by considering coordinated transitions between all

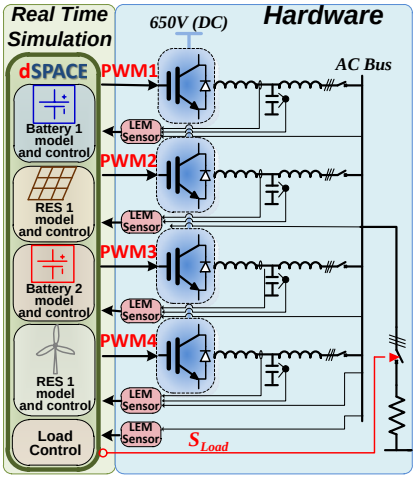

Fig. 17: Scheme of the Experimental Setup.

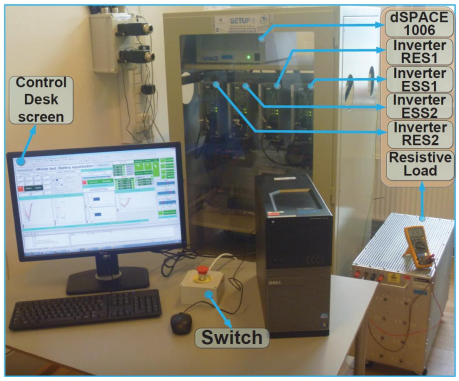

Fig. 18: Experimental Setup at the laboratory.

TCMs and the cooperative behaviours between grid-forming units. Fig. 19 shows: (a) the voltages of the batteries V_{bat1} and V_{bat2}, (b) the SoC values, (c) the Error in the SoCs defined as: $(Error(\%) = SoC_{Bat2} - SoC_{Bat1})$, (d) the active power shared by each ESS (P_{Bat1} and P_{Bat2}), (e) and (f) show the maximum power (P_{MPPTi}) and the generated power (P_{Resi}) for RES1 and RES2 respectively, (g) shows the load consumption profile, and (h) shows the reactive power managed by all the DERs Q_{ESS1}, Q_{ESS2}, Q_{Res1}, and Q_{Res2}.

Fig. 20 shows the voltage amplitude and frequency profiles for the experiment shown in Fig. 19. Here, it is possible to evidence the operation of the bus signalling method, where the frequency deviation is almost negligible in steady state and only transitory perturbations will trigger the changes in the DERs, and the voltage amplitude varies in accordance to the TCM of the microgrid.

From t_0 to t_1: the microgrid operates in TCM1, since the batteries are partially charged (initial SoCs of (75%) and (85%) for ESS1 and ESS2 respectively) and the generation from RESs is $P_{MPPT1} = P_{MPPT2} = 0W$. During this period, the batteries will be discharged for supporting the load consumption. Fig. 19(d) shows how the power shared between ESSs is adjusted for equalizing the SoCs.

At t_1: the maximum available power from RESs are increased ($P_{MPPT1} = 500W$ and $P_{MPPT2} = 250W$). Since generation is larger than consumption the batteries start to be charged and the microgrid continues in TCM1.

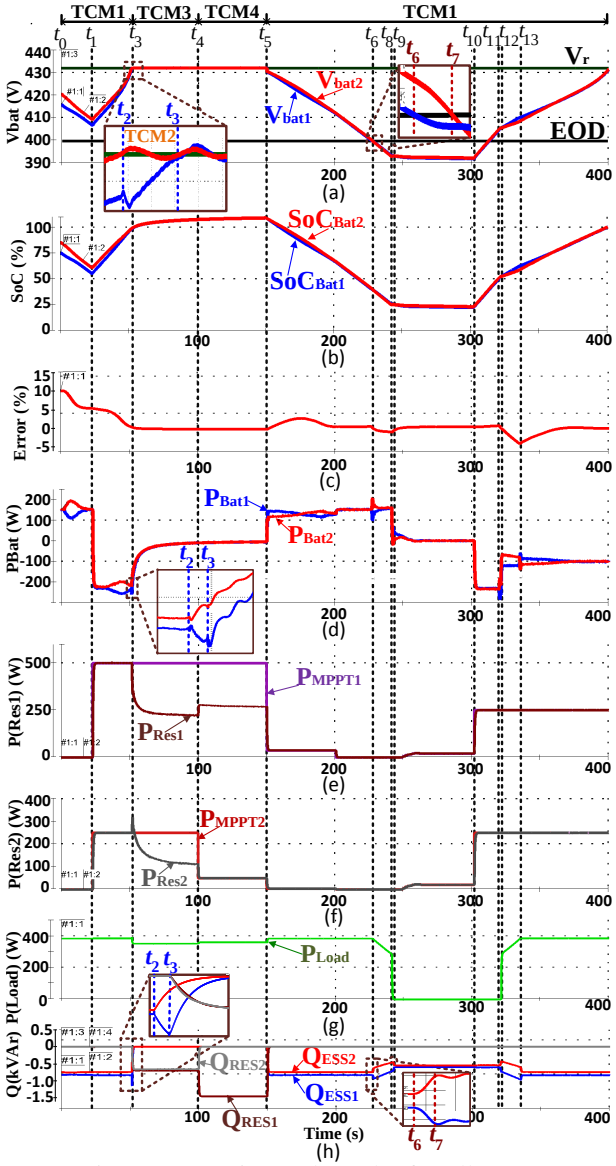

Fig. 19: Experimental results for all TCM.

From t_1 to t_3 it is possible to see how the power sharing is adjusted between the grid-forming units (ESSs) for equalizing the SoCs. Additionally, Fig. 20 shows that the voltage amplitude in the common coupling point (V_{PCC}) is bigger than the nominal voltage E_{nom}, which indicates that ESSs are the current responsible for forming the islanded system ($Co_1 = 1$) in accordance with the proposed signalling strategy.

At t_2: ESS2 reaches the regulation voltage V_r, then, it changes its operation mode to CCM (this time can be seen in the zoom in boxes in Figs. 19 and 20). Consequently, the microgrid changes its topology from TCM1 to TCM2. From t_2 to t_3 ESS1 will be the single unit in the forming task, then, its rate of charge increases and it will assume the managing of all the reactive power (Q). Meanwhile, the reactive power in ESS2 approaches the reference value $(Q^* = 0)$ as can be seen in the zoom-in box of Fig. 19(h). Thanks to the SoC equalization process, the operation of the microgrid under TCM2 is short and the transition in both ESSs is almost simultaneous as can be seen in the long time scale.

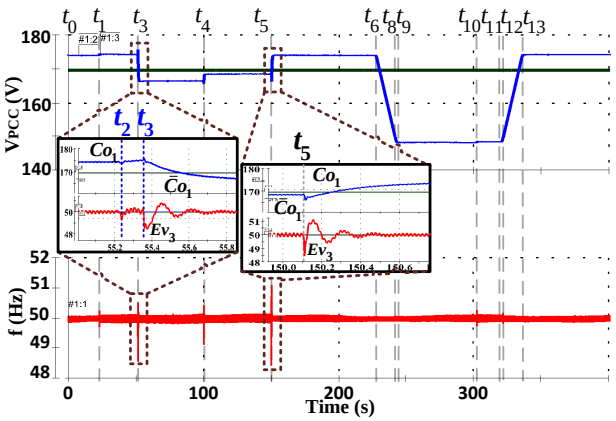

Fig. 20: Common Bus Voltage and Frequency.

At t_3: ESS1 also reaches the regulation voltage V_r, then, the microgrid changes its configuration to the TCM shown in Fig. 3. As a consequence, the frequency drops until the minimum limit of the NDZ as can be seen in Fig. 20 where the event Ev_3 is configured. Also, at the time that event Ev_3occurs $V_{PCC} > E_{nom}$ ($Co_1 = 1$), which means that only RESs will assume the grid-forming control (Fig. 9b).

From t_3 to t_4: it is possible to see how the power is shared between RESs proportionally to their corresponding maximum available power. To be more precise, $P_{Res1} > P_{Res2}$ because $P_{MPPT1} > P_{MPPT2}$. This cooperative behaviour is achieved by the action of the weighting factor $W(P_{MPPT})$. Additionally, in Figs. 19(d) and 19(a) it is possible to see that the power consumption of the ESSs is reduced exponentially in order to keep the voltage of the batteries at a constant value. After t_3 the batteries will enter in a saturation stage in which more than 100% of the energy is returned to the battery for compensating energy losses during the charging stage. This overcharge during the saturation stage is recommended by manufacturers (see Fig. 19(b)) [7]. Meanwhile. Fig. 20 shows that the voltage at the common bus is reduced below the nominal voltage ($V_{PCC} < E_{nom}$), which means ($Co_1 = \bar{C}o_1 = 0$) in accordance to the proposed signalling strategy.

At t_4: P_{MPPT2} is reduced to 50 W ,then, RES2 changes its control from grid-forming to grid-following, since $P_{MPPT2} < P_{Res2}$ (event Ev_2). As a result, the microgrid changes its topology to $TCM4$and RES1 assumes the forming task of the local power grid and the management of the reactive power. Since the grid-following units do not contribute with reactive power managing ($Q^* = 0$), the grid-forming units will be responsible for managing the reactive power consumed by the filter capacitors. Because of that, the grid-forming units will see a capacitive reactive power. From t_4 to t_5 RES1 manages all the reactive power, which is close to the maximum value $Q_{max} = -1500$ VAr (Figs. 19(h)). Then, the voltage in the common coupling point increases due to the reactive current flowing through L_2 as can be seen in Fig. 20. However, the voltage is kept below the nominal value thanks to the adjustment value E_{adj} added in equation (3).

At t_5: $P_{MPPT1} = P_{MPPT2} = 0W$, then, $P_{MPPT1} < P_{Res1}$ (event Ev_2) and RES2 changes to grid-following control. As a consequence, all the DERs will be in CCM (Fig. 3). Fig. 20 shows the transitions for voltage amplitude and frequency after Ev_3. As can be seen at Ev_3 the voltage $V_{PCC} < E_{nom}$ ($\bar{C}o_1$), which means that only the ESSs will assume the grid-forming role and the microgrid returns to $TCM1$. From t_5 to t_6, it is possible to see the effect of circulating currents which increase the Error value temporarily. The circulating currents appear due to differences in the grid-forming units at the time they are connected in parallel [48]. The difference appears because the ESSs are not completely equalized and the open circuit voltages of the batteries are nor the same. In this case, larger differences will cause larger circulating currents after t_5 [37]. Nevertheless, the SoC equalization based on FIS manages to reduce the Error value.

At t_6: the ESSs reach the EOD value almost at the same time due to the equalization. However, because of small differences in the battery voltages of the ESSs (t_6 to t_7 in the zoom in box of Fig. 19(a)), the reduction in the reference voltage E^* is not performed exactly at the same time. This fact causes differences in the reactive power sharing as can be seen in Fig. 19(h) due to the action of $(Q - E)$ droop control loops. From t_6 to t_9 the common bus voltage (V_{PCC}) is reduced as can be seen in Fig. 20. Finally, at t_8 the load is disconnected (see Fig. 19(g) where $P_{Load} = 0$), and in t_9 the reference value, in both ESSs, reaches its minimum value $(E^* = 0.85E_{nom})$ and the voltage in the common bus stops its reduction as can be seen in Fig. 20(g).

At t_{10}: The maximum available power from RESs is increased $(P_{Res1} = P_{Res2} = 250W)$, and the ESSs begin to be charged until t_{11} where SoCs will be equal to 50%. At this point, the reference value starts its restoration (see Fig. 20.) and consequently the common bus voltage increases. Similarly to the voltage reduction process, small differences in the SoC values cause small deviations in the reactive power sharing. Here is where the SoC equalization takes importance since larger differences in the charging and discharging profiles cause larger differences in the reactive power sharing.

At t_{12}: the amplitude in the common bus is greater than the 90% of its nominal value. Therefore, the load is connected, and the reference value E^* continues its restoration until t_{13}.

In the real implementation, it is not possible to ensure equal parameters for all the inverters. For that reason, in Fig. 19(h) shows that the reactive power flow Q is not equally shared between grid-forming units during TCM1 and TCM3. To solve this problem cooperative behaviours can be defined in order to adjust the reactive power sharing in future works. Another important point to highlight is that the SoC equalization allows unifying the charge and discharge profiles for the distributed ESSs. Therefore from a coordination point of view, the distributed ESSs can be seen as a single aggregated one. This fact can be seen in the voltage and SoC profiles in Figs. 19(a) and 19(b).

B. Experiment 2.

The experimental results presented in the Fig. 21 compare the performance of the proposed voltage/frequency signalling when the grid-forming units have to deal with a capacitive reactive power (Fig. 21a) or an inductive reactive power (Fig.

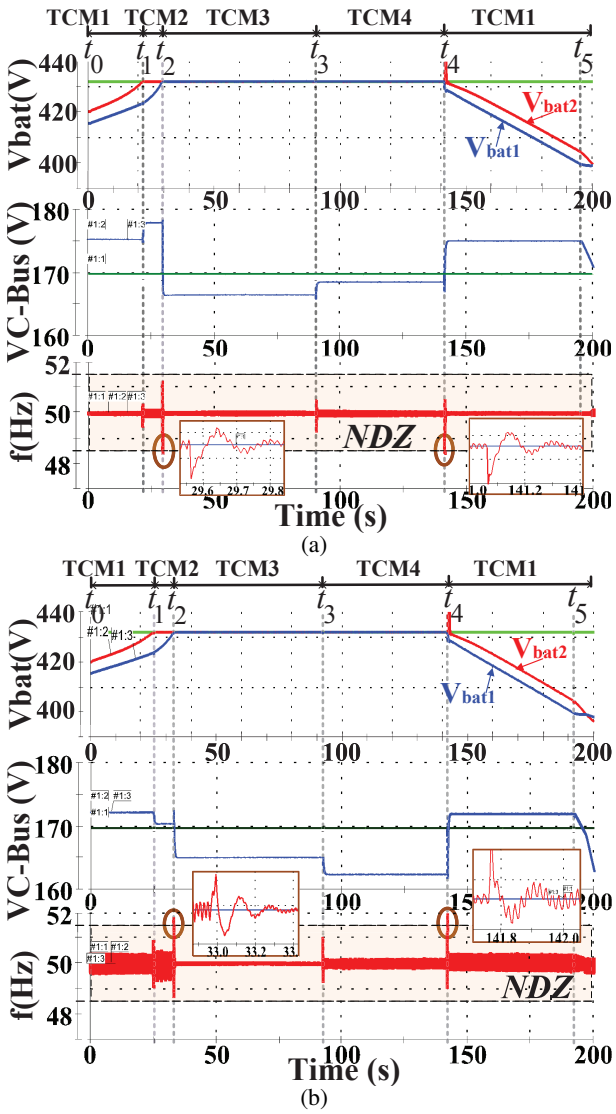

Fig. 21: Voltage/Frequency Signalling (a) Capacitive load, (b) Inductive Load.

21b). The proposed $(Q-E)$ droop characteristic is designed for setting the voltage in the common point above the nominal value when the ESSs are the grid forming units, and setting the voltage bellow the nominal value when the RESs are the grid-forming units in accordance to Fig. 7. The most critical case is presented when only one DER has to assume the grid forming role (TCM2 and TCM4). To have a clearer appreciation about the operation in TCM2, the equalization function has been deactivated for the experiments in Fig. 21. Figs. 21 show the voltages of the batteries V_{bat1} and V_{bat2}, the voltage in the common bus and the frequency in the islanded system. The initial SoC values are set in 75% for ESS1 and 85% for ESS2.

From t_0 to t_1 both ESSs are being charged (TCM1) until t_1 where ESS2 reaches the regulation voltage V_r, and ESS1 becomes the only unit in the grid-forming function. From t_1 to t_2 the microgrid operates in TCM2 and ESS1 has to deal with all the reactive power. In Fig. 21a the voltage increases due to the capacitive reactive power, while in Fig. 21b the common bus voltage drops due to the inductive reactive power. Nevertheless, the proposed $(Q-E)$ droop keep the voltage above the nominal value. At t_2 ESS1 reaches the regulation voltage, and from this point, the RESs have to assume the grid-forming task. During the transitory stage, there is a frequency fluctuation that will trigger the transition of RESs from CCM to VCM. It is possible to appreciate differences in the frequency fluctuation between the capacitive and inductive cases. While in the capacitive case the frequency tends to drop, in the inductive case the frequency tends to increases. Because of that, in the capacitive case, the event Ev_3 is configured when the frequency reached the minimum limit of the NDZ, while for the inductive case the event Ev_3 is configured when the frequency reached the maximum limit of the NDZ.

From t_2 to t_4 the RESs assume the grid-forming function. From t_2 to t_3 both RESs share the active and reactive power by means of the droop control loops (TCM3). At t_3 RES2 is not able to continue with the current power-sharing and changes its control from grid-forming to grid-following. Then, RES1 assumes solely the grid-forming role and consequently the control of the reactive power (TCM4). As before, in the capacitive case (Fig. 21a) the voltage in the common bus increases, while in the inductive case (Fig. 21b) the voltage in the common bus decreases. At t_4 the frequency fluctuation triggers the transition from TCM4 to TCM1, and similarly to t_2, in the capacitive case the event is triggered by the minimum limit of the NDZ, while in the capacitive case the event is triggered by the maximum limit of the NDZ. At t_4 there is a small overshoot in V_{bat2} caused by circulating currents since the ESSs are not equalized [37]. It is possible to see that the adjustment value E_{adj} is required for keeping the common bus voltage above the nominal value when ESSs are the grid-forming units (t_1 to t_2 in Fig. 21b), and bellow the nominal value when RESs are the grid-forming units (t_3 to t_4 in Fig. 21a). As explained before, the value of E_{adj} depends of the maximum value of the reactive power Q_{max} and the value of the output inductor L_2.

C. Experiment 3.

The experiment in Fig. 22 emulates the performance of the microgrid in a time horizon of 24 hours. In order to speed-up the time of the experiment, the time has been scaled down considering a time base in which 1 hour of generation in the real profile is run in 60 seconds during the experiment. Therefore, a generation profile of 24 hours corresponds to 1440 seconds in the experiment. Fig. 22 shows: (a) the voltage of the batteries, (b) the SoC values, (c) the Error value, (d) the active power shared by the ESSs, (e) the generation profile from RES1, (f) and the generation profile of RES2. The experiment in Fig. 22 also shows the performance of the microgrid when ESS and RES are put off-line. Initially, the SoCs in both ESSs are equalized at 80% and a constant load of 188 W is considered.

At t_1: ESS1 is put off-line, then, ESS2 assume solitary the grid-forming control and the power balance in the microgrid. From t_1 to t_2 it is possible to see that the battery voltage (V_{bat1}) and the SoC (SoC_{Bat1}) of ESS1 remain constant since ESS1 is not participating in the operation of the microgrid. Meanwhile, ESS2 will be the only unit responsible

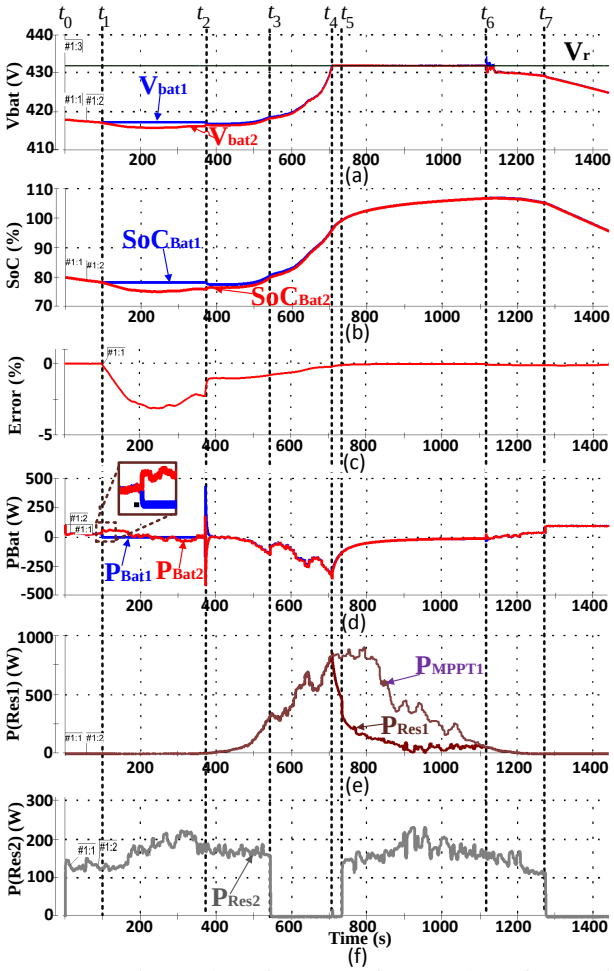

Fig. 22: Experimental Performance for one day of operation.

for managing the power balance in the system, and it will move from charge to discharge since the load consumption is approximately 180W and the generation from the WT is varying around this value.

At t_2: ESS1 is connected and instantaneous circulating currents appear due to the parallel connection of grid-forming units as can be seen in Fig. 22(d) [48]. At t_3: RES2 is put off-line and the power balance task performed by the ESS is correspondingly adjusted.

At t_4: The ESSs reach the regulation value (V_r) almost simultaneously and RES1 adopts solitary the grid-forming control since its available power is larger than the consumption. It is possible to see that the SoCs are equalized after the difference caused by the temporal disconnection of ESS1.

At t_5: RES2 is re-connected in CCM, then, the generation from RES1 is correspondingly adjusted, while the ESSs continue in constant voltage regulation, since the available power is larger than the consumption.

At t_6: the generation becomes lower than consumption and the ESSs re-assume the grid-forming control, as a consequence, the microgrid changes its operation to TCM1. Finally, at t_7 RES2 is turned off and the consumption is supplied only by the ESSs.

The experiment in Fig. 22 shows the plug-and-play capability of the proposed strategy since the microgrid is able to continue operating even when some units are put off-line or are integrated.

VIII. Conclusions

This paper proposes a coordination architecture for a microgrid based on DERs integrated into a network configuration. The proposed strategy rely on distributed decision-making units that execute simple rules and actions to coordinate the operation of DERs in accordance with information obtained from a voltage-frequency bus-signalling method at the common coupling point. Therefore, the proposed method relies only on local measurements and actions without the use of additional communication channels. The proposed strategy considers proper dynamic behaviour and reliable operation modes for the islanded power system. Additionally, the proposed architecture considers different stages and limits for a proper charging of ESSs based on batteries, which end up being the main conditions to define the coordination architecture. On top of that, the proposed coordination strategy includes cooperative operations such as SoC equalization and proportional power curtailment, which are also addressed without the use of external communication. The equalization of the charging profiles for distributed ESSs allows an easy definition of the coordination architecture since their coordination actions will be performed simultaneously resembling coordination of a microgrid with a single aggregated ESS.

By itself, the proposed coordination strategy has the inherent characteristics of a distributed strategy such as modularity, plug-and-play capability, scalability, and expandability. Nevertheless, the expandability in a network configuration -such as the one considered for the case study- is limited compared with a radial configuration which allows the integration along long feeders. However, a radial configuration increases the problems related to power flow and voltage quality along the feeders which may compromise the operation of the proposed coordination architecture. This fact opens the door for future research regarding additional cooperative behaviours between the DERs which enhance the voltage quality in the connection points along the feeders and allow the deployment of the proposed strategy in radial configurations.

References

[1] J. de Matos, F. e Silva, and L. Ribeiro, "Power control in ac isolated microgrids with renewable energy sources and energy storage systems," *IEEE Transactions on Industrial Electronics,*, vol. 62, no. 6, pp. 3490–3498, 2015.

[2] B. Heap, "Smart villages: New thinking for off-grid communities worldwide," tech. rep., Banson/Smart Villages Initiative., 2015.

[3] M. H. Alsharif, R. Nordin, and M. Ismail, "Energy optimisation of hybrid off-grid system for remote telecommunication base station deployment in malaysia," *EURASIP Journal on Wireless Communications and Networking*, vol. 2015, no. 1, p. 64, 2015.

[4] H. Kanchev, F. Colas, V. Lazarov, and B. Francois, "Emission reduction and economical optimization of an urban microgrid operation including dispatched pv-based active generators," *IEEE Transactions on Sustainable Energy*, vol. 5, pp. 1397–1405, Oct 2014.

[5] J. Pecas Lopes, C. Moreira, and A. Madureira, "Defining control strategies for microgrids islanded operation," *IEEE Transactions on Power Systems*, vol. 21, pp. 916–924, May 2006.

[6] M. Beaudin, H. Zareipour, A. Schellenberg, and W. Rosehart, "Chapter 1 - energy storage for mitigating the variability of renewable electricity sources," in *Energy Storage for Smart Grids* (P. D. Lu, ed.), pp. 1 – 33, Boston: Academic Press, 2015.

[7] "IEEE Guide for Optimizing the Performance and Life of Lead-Acid Batteries in Remote Hybrid Power Systems," *IEEE Std 1561-2007*, pp. C1–25, May 2008.

[8] F. Katiraei, R. Iravani, N. Hatziargyriou, and A. Dimeas, "Microgrids management," *IEEE Power and Energy Magazine*, vol. 6, pp. 54–65, May 2008.

[9] R. Newnham and W. Baldsing, "Advanced management strategies for remote-area power-supply systems," *Journal of Power Sources*, vol. 133, no. 1, pp. 141 – 146, 2004. Proceedings of the Tenth Asian Battery Conference.

[10] W. Shi, X. Xie, C. C. Chu, and R. Gadh, "Distributed optimal energy management in microgrids," *IEEE Transactions on Smart Grid*, vol. 6, pp. 1137–1146, May 2015.

[11] C. Wang, M. Liu, and L. Guo, "Cooperative operation and optimal design for islanded microgrid," in *2012 IEEE PES Innovative Smart Grid Technologies (ISGT)*, pp. 1–8, Jan 2012.

[12] J. Y. Kim, J. H. Jeon, S. K. Kim, C. Cho, J. H. Park, H. M. Kim, and K. Y. Nam, "Cooperative control strategy of energy storage system and microsources for stabilizing the microgrid during islanded operation," *IEEE Transactions on Power Electronics*, vol. 25, pp. 3037–3048, Dec 2010.

[13] X. Lu, K. Sun, J. Guerrero, J. Vasquez, and L. Huang, "State-of-charge balance using adaptive droop control for distributed energy storage systems in dc microgrid applications," *IEEE Transactions on Industrial Electronics*, vol. 61, pp. 2804–2815, June 2014.

[14] E. Serban and H. Serban, "A control strategy for a distributed power generation microgrid application with voltage- and current-controlled source converter," *IEEE Transactions on Power Electronics*, vol. 25, pp. 2981–2992, Dec 2010.

[15] H. Mahmood, D. Michaelson, and J. Jiang, "Strategies for independent deployment and autonomous control of pv and battery units in islanded microgrids," *IEEE Journal of Emerging and Selected Topics in Power Electronics*, vol. 3, pp. 742–755, Sept 2015.

[16] M. Mao, H. Huang, and L. Chang, "Real-time energy coordinated and balance control strategies for microgrid with photovoltaic generators," in *4th IEEE International Symposium on Power Electronics for Distributed Generation Systems (PEDG)*, pp. 1–7, July 2013.

[17] D. Wu, F. Tang, T. Dragicevic, J. Vasquez, and J. Guerrero, "Autonomous active power control for islanded ac microgrids with photovoltaic generation and energy storage system," *IEEE Transactions on Energy Conversion*, vol. 29, pp. 882–892, Dec 2014.

[18] W.-Y. Chang, "The state of charge estimating methods for battery: A review," *ISRN Applied Mathematics*, 2013. Copyright - Copyright 2013 Wen-Yeau Chang. Wen-Yeau Chang et al. This is an open access article distributed under the Creative Commons Attribution License, which permits unrestricted use, distribution, and reproduction in any medium, provided the original work is properly cited; Last updated - 2015-02-19.

[19] J. Cui, K. Li, Y. Sun, Z. Zou, and Y. Ma, "Distributed energy storage system in wind power generation," in *2011 4th International Conference on Electric Utility Deregulation and Restructuring and Power Technologies (DRPT)*, pp. 1535–1540, July 2011.

[20] F. Marra, G. Yang, C. Traeholt, J. Ostergaard, and E. Larsen, "A decentralized storage strategy for residential feeders with photovoltaics," *IEEE Transactions on Smart Grid*, vol. 5, pp. 974–981, March 2014.

[21] D. Wu, F. Tang, T. Dragicevic, J. Vasquez, and J. Guerrero, "A control architecture to coordinate renewable energy sources and energy storage systems in islanded microgrids," *IEEE Transactions on Smart Grid*, vol. 6, pp. 1156–1166, May 2015.

[22] T. Dragičević, J. M. Guerrero, J. C. Vasquez, and D. Škrlec, "Supervisory control of an adaptive-droop regulated dc microgrid with battery management capability," *IEEE Transactions on Power Electronics*, vol. 29, pp. 695–706, Feb 2014.

[23] N. L. Díaz, T. Dragičević, J. C. Vasquez, and J. M. Guerrero, "Intelligent distributed generation and storage units for dc microgrids - a new concept on cooperative control without communications beyond droop control," *IEEE Transactions on Smart Grid*, pp. 2476–2485, Sept 2014.

[24] T. Dragičević, J. M. Guerrero, and J. C. Vasquez, "A distributed control strategy for coordination of an autonomous lvdc microgrid based on power-line signaling," *IEEE Transactions on Industrial Electronics*, vol. 61, pp. 3313–3326, July 2014.

[25] T. Vandoorn, J. Vasquez, J. De Kooning, J. Guerrero, and L. Vandevelde, "Microgrids: Hierarchical control and an overview of the control and reserve management strategies," *IEEE Industrial Electronics Magazine*, vol. 7, pp. 42–55, Dec 2013.

[26] I. Buchmann and C. E. Inc, *Batteries in a Portable World: A Handbook on Rechargeable Batteries for Non-engineers*. Cadex Electronics, 4th edition ed., 2016.

[27] D. Linden and T. Reddy, *Handbook of Batteries*. McGraw-Hill handbooks, McGraw-Hill Education, third edition ed., 2001.

[28] J. Rocabert, A. Luna, F. Blaabjerg, and P. Rodríguez, "Control of power converters in ac microgrids," *IEEE Transactions on Power Electronics*, vol. 27, pp. 4734–4749, Nov 2012.

[29] N. L. Díaz, E. A. Coelho, J. C. Vasquez, and J. M. Guerrero, "Stability analysis for isolated ac microgrids based on pv-active generators," in *2015 IEEE Energy Conversion Congress and Exposition (ECCE)*, pp. 4214–4221, Sept 2015.

[30] J. Guerrero, L. Garcia De Vicuna, J. Matas, M. Castilla, and J. Miret, "A wireless controller to enhance dynamic performance of parallel inverters in distributed generation systems," *IEEE Transactions on Power Electronics*, vol. 19, pp. 1205–1213, Sept 2004.

[31] S. Liu, S. Zhuang, Q. Xu, and J. Xiao, "Improved voltage shift islanding detection method for multi-inverter grid-connected photovoltaic systems," *IET Generation, Transmission Distribution*, vol. 10, no. 13, pp. 3163–3169, 2016.

[32] A. Khamis, H. Shareef, E. Bizkevelci, and T. Khatib, "A review of islanding detection techniques for renewable distributed generation systems," *Renewable and Sustainable Energy Reviews*, vol. 28, pp. 483 – 493, 2013.

[33] X. S. Zhou, Y. J. Ma, and J. R. Wu, "A review of islanding detection method of grid-connected pv power system," in *Advances in Power and Electrical Engineering*, vol. 614 of *Advanced Materials Research*, pp. 815–818, Trans Tech Publications, 2 2013.

[34] E. C. for Electrotechnical Standardization, "Voltage characteristics of electricity supplied by public distribution systems," *Std EN 50160*, no. EN 50160, 2005.

[35] S. Golestan and J. M. Guerrero, "Conventional synchronous reference frame phase-locked loop is an adaptive complex filter," *IEEE Transactions on Industrial Electronics*, vol. 62, pp. 1679–1682, March 2015.

[36] S. Golestan, M. Monfared, F. D. Freijedo, and J. M. Guerrero, "Performance improvement of a prefiltered synchronous-reference-frame pll by using a pid-type loop filter," *IEEE Transactions on Industrial Electronics*, vol. 61, pp. 3469–3479, July 2014.

[37] N. Díaz, D. Wu, T. Dragicevic, J. Vasquez, and J. Guerrero, "Stored energy balance for distributed pv-based active generators in an ac microgrid," in *2015 IEEE Power Energy Society General Meeting*, pp. 1–5, July 2015.

[38] Y. Zhang, H. J. Jia, and L. Guo, "Energy management strategy of islanded microgrid based on power flow control," in *2012 IEEE PES Innovative Smart Grid Technologies (ISGT)*, pp. 1–8, 2012.

[39] H. Kakigano, Y. Miura, and T. Ise, "Distribution voltage control for dc microgrids using fuzzy control and gain-scheduling technique," *IEEE Transactions on Power Electronics*, vol. 28, pp. 2246–2258, May 2013.

[40] C. Li, T. Dragicevic, M. Garcia Plaza, F. Andrade, J. Vasquez, and J. Guerrero, "Multiagent based distributed control for state-of-charge balance of distributed energy storage in dc microgrids," in *40th Annual Conference of the IEEE Industrial Electronics Society, (IECON)*, pp. 2180–2184, Oct 2014.

[41] O. Palizban and K. Kauhaniemi, "Distributed cooperative control of battery energy storage system in {AC} microgrid applications," *Journal of Energy Storage*, vol. 3, pp. 43 – 51, 2015.

[42] X. Lu, K. Sun, J. Guerrero, J. Vasquez, and L. Huang, "Double-quadrant state-of-charge-based droop control method for distributed energy storage systems in autonomous dc microgrids," *IEEE Transactions on Smart Grid*, vol. 6, pp. 147–157, Jan 2015.

[43] Z. Miao, L. Xu, V. Disfani, and L. Fan, "An soc-based battery management system for microgrids," *IEEE Transactions on Smart Grid*, vol. 5, pp. 966–973, March 2014.

[44] T. Kim and W. Qiao, "A hybrid battery model capable of capturing dynamic circuit characteristics and nonlinear capacity effects," *IEEE Transactions on Energy Conversion*, vol. 26, pp. 1172–1180, Dec 2011.

[45] E. Coelho, P. Cortizo, and P. Garcia, "Small-signal stability for parallel-connected inverters in stand-alone ac supply systems," *IEEE Transactions on Industry Applications*, vol. 38, pp. 533–542, Mar 2002.

[46] K. Aström and R. Murray, *Feedback Systems: An Introduction for Scientists and Engineers*. Princeton University Press, 2010.

[47] J. M. Kwon, K. H. Nam, and B. H. Kwon, "Photovoltaic power conditioning system with line connection," *IEEE Transactions on Industrial Electronics*, vol. 53, pp. 1048–1054, June 2006.

[48] X. Wang, F. Blaabjerg, and Z. Chen, "An improved design of virtual output impedance loop for droop-controlled parallel three-phase voltage source inverters," in *IEEE Energy Conversion Congress and Exposition (ECCE)*, pp. 2466–2473, Sept 2012.

Nelson L. Díaz (S'09-M'17) received the B.S degree in Electronic Engineering from the Universidad Distrital F.J.C in 2008, the M.S. degree in Industrial Automation from the Universidad Nacional de Colombia in 2011, Bogotá, Colombia, and the Ph.D. degree in Energy Technology from Aalborg Universit of Denmark in 2017 as part of the Microgrids Research Program. Currently, he is Assistant Professor at the Engineering Faculty of Universidad Distrital F.J.C. of Bogotá Colombia. He is a member of the Research Laboratory of Alternative Energy Sources, Universidad Distrital F.J.C. His current research interests include microgrids and power converters control.

Juan C. Vasquez (M'12-SM'14) received the B.S. degree in electronics engineering from the Autonomous University of Manizales, Manizales, Colombia, and the Ph.D. degree in automatic control, robotics, and computer vision from the Technical University of Catalonia, Barcelona, Spain, in 2004 and 2009, respectively. He was with the Autonomous University of Manizales working as a teaching assistant and the Technical University of Catalonia as a Post-Doctoral Assistant in 2005 and 2008 respectively. In 2011, he was Assistant Professor and from 2014 he is working as an Associate Professor at the Department of Energy Technology, Aalborg University, Denmark where he is the Vice Programme Leader of the Microgrids Research Program (see microgrids.et.aau.dk). From Feb. 2015 to April. 2015 he was a Visiting Scholar at the Center of Power Electronics Systems (CPES) at Virginia Tech and a visiting professor at Ritsumeikan University, Japan. His current research interests include operation, advanced hierarchical and cooperative control, optimization and energy management applied to distributed generation in AC/DC Microgrids, maritime microgrids, advanced metering infrastructures and the integration of Internet of Things and Cyber-Physical Systems into the SmartGrid. He has more than 100 technical papers only in Microgrids in international IEEE conferences and journals.

Dr. Vasquez is currently a member of the IEC System Evaluation Group SEG4 on LVDC Distribution and Safety for use in Developed and Developing Economies, the Renewable Energy Systems Technical Committee TC-RES in IEEE Industrial Electronics, PELS, IAS, and PES Societies.

Josep M. Guerrero (S'01-M'04-SM'08-FM'15) received the B.S. degree in telecommunications engineering, the M.S. degree in electronics engineering, and the Ph.D. degree in power electronics from the Technical University of Catalonia, Barcelona, in 1997, 2000 and 2003, respectively. Since 2011, he has been a Full Professor with the Department of Energy Technology, Aalborg University, Denmark, where he is responsible for the Microgrid Research Program. From 2012 he is a guest Professor at the Chinese Academy of Science and the Nanjing University of Aeronautics and Astronautics; from 2014 he is chair Professor in Shandong University; from 2015 he is a distinguished guest Professor in Hunan University; and from 2016 he is a visiting professor fellow at Aston University, UK. His research interests is oriented to different microgrid aspects, including power electronics, distributed energy-storage systems, hierarchical and cooperative control, energy management systems, smart metering and the internet of things for AC/DC microgrid clusters and islanded minigrids; recently specially focused on maritime microgrids for electrical ships, vessels, ferries and seaports. Prof. Guerrero is an Associate Editor for the IEEE TRANSACTIONS ON POWER ELECTRONICS, the IEEE TRANSACTIONS ON INDUSTRIAL ELECTRONICS, and the IEEE Industrial Electronics Magazine, and an Editor for the IEEE TRANSACTIONS on SMART GRID and IEEE TRANSACTIONS on ENERGY CONVERSION. He has been Guest Editor of the IEEE TRANSACTIONS ON POWER ELECTRONICS Special Issues: Power Electronics for Wind Energy Conversion and Power Electronics for Microgrids; the IEEE TRANSACTIONS ON INDUSTRIAL ELECTRONICS Special Sections: Uninterruptible Power Supplies systems, Renewable Energy Systems, Distributed Generation and Microgrids, and Industrial Applications and Implementation Issues of the Kalman Filter; the IEEE TRANSACTIONS on SMART GRID Special Issues: Smart DC Distribution Systems and Power Quality in Smart Grids; the IEEE TRANSACTIONS on ENERGY CONVERSION Special Issue on Energy Conversion in Next-generation Electric Ships. He was the chair of the Renewable Energy Systems Technical Committee of the IEEE Industrial Electronics Society. He received the best paper award of the IEEE Transactions on Energy Conversion for the period 2014-2015. In 2014 and 2015 he was awarded by Thomson Reuters as Highly Cited Researcher, and in 2015 he was elevated as IEEE Fellow for his contributions on "distributed power systems and microgrids".